Proceedings of ASME Turbo Expo 2025
Turbomachinery Technical Conference and Exposition
GT2025
June 16-20, 2025, Memphis, Tennessee, USA

GT2025-152020

LES OF HYDROGEN-FUELLED COMBUSTION IN THE FIRST STAGE OF THE ANSALDO ENERGIA GT36 CONSTANT PRESSURE SEQUENTIAL COMBUSTION SYSTEM

Aldo Schioppa[1,*], Luis Tay-Wo-Chong[2], Andrea Ciani[2], Laurent Gicquel[1]

[1]CERFACS, Toulouse, France
[2]Ansaldo Energia Switzerland AG, Baden, Switzerland

ABSTRACT

Sequential combustion systems have demonstrated outstanding fuel flexibility, thus constituting an effective solution for burning hydrogen-based fuels at low emissions. The EU- and Swiss-funded FLEX4H2 project is leveraging sequential combustion advantages to enable operation with either pure methane, pure hydrogen or methane-hydrogen blends. The development focuses on the Ansaldo GT36 engine utilising a Constant Pressure Sequential Combustion (CPSC) system. In such a system the first stage generates the required inlet temperature to stabilise the second stage flame by self-ignition, providing an additional degree of freedom to accommodate changes in fuel reactivity while limiting emissions. The static and dynamic stability of the system is a key element of the development aiming at stable combustion across various operating conditions and ranges of fuels. Typically, varying the fuel composition from 0% to 100% of hydrogen has an important impact on the first stage flame stability and acoustic response. To investigate such possibilities a priori, numerical simulations—specifically Large Eddy Simulations—of the multi-burner first stage are performed for different blend ratios. These simulations provide valuable insights into the flame's statistically stationary behaviour, anchoring and morphology. In the following, recent advancements in the Thickened Flame (TF) model for hydrogen flames and multi-fuels injection are specifically applied to this industrial configuration, demonstrating its effectiveness in capturing hydrogen's impact on the system.

Keywords: LES, Hydrogen, Combustion

NOMENCLATURE

Roman letters

K_{inlet}	Relaxation Coefficient at Inlet
K_{outlet}	Relaxation Coefficient at Outlet
m_{fuel}	Total Mass Flow Rate of Fuel
$\dot{q}$	Volumetric Heat Release
R	Thermal Resistance
R_{inlet}	Reflection Coefficient at Inlet
T	Static Temperature
T_{ad}	Adiabatic Temperature
T_{ref}	Reference Temperature (Heat Losses)
T_{u}	Reactants Temperature
(U_x, U_y, U_z)	Velocity Vector
U_0	Average Velocity Magnitude at Lance Pilot End Plane
X_k	Volume Fraction of Species k

Greek letters

$\dot{\omega}_k$	Source Term of Species k
ϕ	Equivalence Ratio
Θ	Normalised Temperature

Superscripts

$*$	Non-dimensional Quantity

Acronyms

ARC	Analytically Reduced Chemistry
CBB	Center-Body Burner
CPSC	Constant Pressure Sequential Combustion
ISL	Inner Shear Layer
IRZ	Inner Recirculation Zone
LES	Large Eddy Simulation
MBFS	Multi-Burner First Stage
MET	Mixer Exit Temperature
OSL	Outer Shear Layer
ORZ	Outer Recirculation Zone
PFR	Pilot-to-Fuel Ratio
QSS	Quasi-Steady Species
RANS	Reynolds Averaged Navier-Stokes
TD	Thermo-Diffusive
TFLES	Thickened Flame Model

1. INTRODUCTION

As awareness of climate change grew, reducing fossil fuel use became a priority, challenging gas turbine producers to reduce CO_2 emissions while maintaining the efficiency of their ma-

*Corresponding author: schioppa@cerfacs.fr

chines. The energy market's shift toward renewables also meant that turbines had to handle fluctuating grid demands. This shift led to the need for turbines that could operate on carbon-free fuels like hydrogen, while still being able to work with natural gas or fuel blends. Although the goals of reducing NO_x and CO emissions remain, handling a wide range of fuel reactivities—particularly with respect to autoignition delay time and flame speed [1, 2]—presents challenges in maintaining combustion stability and avoiding flashback, as well as in dealing with the extension of lean blow-off and flammability limits [3]. From a practical perspective, hydrogen enrichment modifies the flame shape [4] and the heat release rate distribution in more complex swirl-stabilised flames [5], which in turn modifies the flame acoustic response [6]. Therefore, efforts are not only focused on improving current gas turbine designs to meet stringent air pollution standards, but also on adapting them to cope with the wider ranges of flame speed and reactivity introduced by the use of hydrogen blends, as well as different thermo-acoustic coupling and system stabilisation. From a numerical standpoint, Large Eddy Simulation has proven to be a highly effective tool for studying reacting flows [7], and in capturing flame morphology and stabilisation mechanisms in statistically steady regimes [8]. For this reason, LES is employed in this paper to evaluate the statistically stationary flame behaviour of Ansaldo GT36 first stage at ambient pressure, marking an improvement over previous simulations that relied on the RANS approach [9]. Various operating conditions at atmospheric pressure and different blend ratios are simulated. Although these conditions are not strictly (engine) iso-power, valuable insights can still be gained, particularly concerning the mechanisms of flame stabilisation when hydrogen is introduced. Furthermore, the results obtained here and their analysis represent initial and essential steps toward studying the acoustic response of the burner under different blend ratios, as well as potentially laying the groundwork for high-pressure LES at similar conditions. The article is structured as follows: the subsequent sections include a short overview on the Ansaldo GT36 engine, followed by a comprehensive description of the simulated cases and LES numerical setup. Finally, the results are discussed.

2. GT36 - BRIEF OVERVIEW

2.1 Constant Pressure Sequential Combustion (CPSC)

For a more comprehensive description of the CPSC concept, readers may refer to [10–13]. The CPSC system in the Ansaldo GT36 gas turbine is engineered for high efficiency, low emissions, and operational flexibility. It comprises two sequential combustion stages: the first stage, known as the Multi-Burner First Stage (MBFS), operates on the principle of turbulent premixed flame propagation [9]. The second stage, referred to as the Center-Body Burner (CBB) [14], achieves flame stabilisation primarily through self-ignition. Between the two combustion stages, a dilution air mixer is incorporated to provide appropriate conditions for autoignition operation of the second stage. Both combustion stages operate at nearly the same pressure. The CPSC minimises NO_x emissions by adjusting the firing temperatures of the first and second stages at different loads. Its flexible fuel staging allows seamless adaptation to varying fuel compositions, ensuring consistent performance despite changes in fuel properties. This paper focuses on the MBFS.

2.2 BEV Burner and Multi-Burner First Stage (MBFS) Combustor

A more thorough presentation about the BEV and MBFS is available in Pennell *et al.* [9]. The BEV burner and MBFS system represent key advancements in gas turbine technology, enabling the GT36 to operate with low emissions, high fuel flexibility, and strong dynamic stability. These components are pivotal in achieving the turbine's goal of reducing carbon emissions and ensuring reliable operation with diverse fuel blends, including hydrogen. The BEV burner, part of the MBFS system, plays a crucial role in stabilising the flame and ensuring efficient fuel-air mixing. It integrates features from previous designs (EV [15] and AEV [16]) and introduces enhancements to meet modern fuel demands, such as hydrogen blending. A central extended lance in the burner stabilises the flame by anchoring at the lance tip. This helps to maintain reaction continuity, even at low loads, which is essential for stable combustion and startup reliability. The BEV burner includes a premixing duct and eight air slots, which enhance fuel-to-air premixing and thereby contribute to low NO_x emissions. The exit diffuser is a notable feature that reduces pressure losses of the burner. The burner design is optimised for hydrogen-methane fuel blends, addressing the challenges of fuel reactivity, flashback stability, and emission control at elevated firing temperatures. The MBFS combustor consists of four BEV burners arranged around a premix igniter. This arrangement allows efficient ignition and flame stabilisation across the full range of operating conditions, from low-load startup to full-load operation. Air is fed to the burners via a convectively cooled liner and an air metering plate, ensuring consistent air distribution across all burners. The liner design enables proper air passage for the sequential burner downstream, ensuring complete combustion and minimal CO emissions even at low loads. The operational flexibility of the MBFS combustor is evident in its fuel staging concept. The combustor allows independent control of fuel to each burner group, with adjustable pilot fuel ratios and Mixer Exit Temperatures (MET, sequential combustor inlet temperature) to optimise combustion dynamics and emissions. The highest firing temperatures occur during low-load conditions to ensure CO burnout, while at full load, the MBFS operates leanly to minimise NO_x emissions. This inverse temperature behaviour enables efficient combustion control across the entire load range.

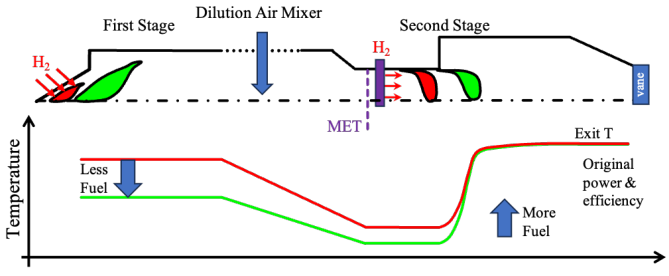

FIGURE 1: TUNING OF TEMPERATURES AND FUEL SPLITS FOR HYDROGEN OPERATION (TAKEN FROM [9]).

An illustration of the MET variation with H_2 content can be found

in [12]. This concept proves highly effective, even for hydrogen blends. Specifically, when hydrogen is introduced, the MET requirement can be further reduced across all loads to account for hydrogen's higher flame speed in the BEV burner and its shorter autoignition time in the CBB (see Fig. 1). As mentioned earlier, since the firing temperature in the MBFS is governed by the required MET, lowering the MET necessitates a reduction in the MBFS firing (flame) temperature. This reduction has the added advantage of decreasing the flame speed, mitigating the risk of flashback, and addressing the challenges posed by hydrogen's high reactivity. Thus, the MBFS operates with varying flame temperatures depending on the hydrogen content. Additionally, as the flame temperature decreases, the pilot-fuel ratio (PFR), defined as the ratio of fuel mass flow in the pilot lance to the total fuel in the burner, is increased with higher hydrogen content to enhance flame stabilisation under reduced temperature conditions.

3. CASES

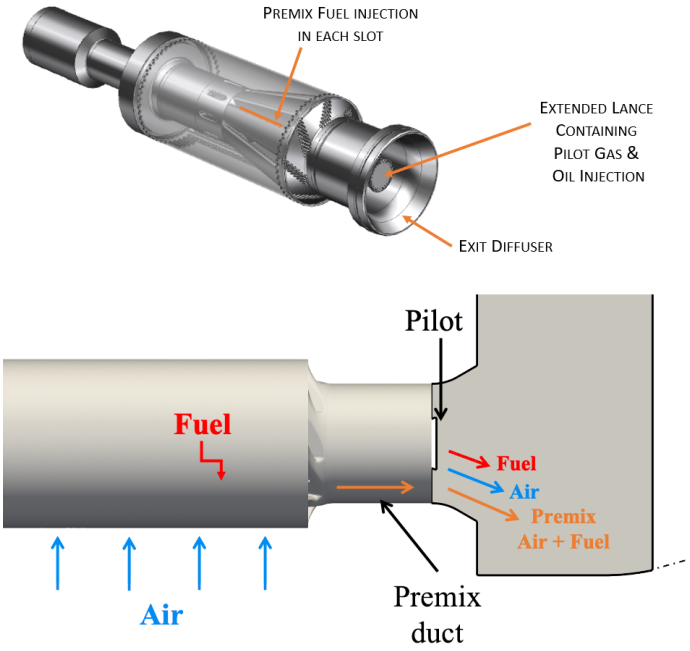

FIGURE 2: (TOP) BEV BURNER (TAKEN FROM [9]) AND (BOTTOM) ITS FUEL AND AIR INJECTION DISTRIBUTION.

Three H_2-blend ratios, corresponding to hydrogen volume fractions of $X_{H_2} = 0$, $X_{H_2} = 0.5$, and $X_{H_2} = 1$, at atmospheric conditions are simulated. Henceforth, they are denoted "CH_4", "CH_4/H_2" and "H_2" cases, respectively. In the BEV burner, there are two fuel injection points: one upstream of the premix duct, described by an equivalent ratio ϕ_{premix}, and another at the pilot (see Fig. 2). Typically, the majority of the fuel is injected upstream of the premix duct, at the swirler, though the proportion of fuel between the latter and the pilot can vary depending on the operating conditions, as indicated in Sec. 2.2. Therefore, three different levels of PFR are set for the three different blends considered in this study with the lowest ratio in the CH_4 case and the highest in the H_2 case. Taking the CH_4/H_2 as a reference, the PFR in the CH_4 case is reduced by more than a factor of 1.5, while in the H_2 case it is increased by a factor higher than 1.5. The selected conditions and fuel splits reflect representative operating conditions of the burner across different hydrogen content, where $\text{MET}_{CH_4} > \text{MET}_{CH_4/H_2} > \text{MET}_{H_2}$. Simulations are performed under varying premix equivalence ratios, with decreasing ϕ_{premix} as the global hydrogen volume fraction increases. This approach prevents excessively high flame temperatures and ensures stable combustion within the CPSC concept.

4. NUMERICAL SETUP

The Favre-filtered, multi-species, reacting Navier-Stokes equations are solved via the massively parallel, time-explicit, fully compressible CERFACS code *AVBP* [17], which has been vastly utilised and validated in the past on both laboratory [18] and industrial [19] burners. The system of LES equations is numerically resolved by relying upon a finite-element approach implemented within a cell-vertex formulation. The convection flux is discretised by using a second-order-accurate Lax-Wendroff scheme [20]. The diffusive flux is discretised using a centred second-order scheme, while the sub-grid stress tensor is modelled via the Smagorinsky sub-grid scale model [21].

4.1 Chemistry and Transport Model

The chemistry is modelled via either detailed chemistry or the 2-steps global mechanism 2S-CH4-BFER [22], depending on the blend ratio. The CH_4/H_2 chemistry is an ARC (Analytically Reduced Chemistry) scheme [23] and comprises 15 species, 256 elementary steps (138 reactions) and 9 Quasi-Steady Species (QSS) (CH4-15-256-9) [24], and is derived from the POLIMI_2003_C1_C3_HT_NOx global mechanism [25], whereas the H_2 chemistry is a sub-set of the San Diego mechanism [26] and encapsulates 9 species and 21 reactions (H2-9-42-0). The choice between a mixture-averaged transport model [27] or a simplified transport model depends on whether an ARC mechanism is employed. In the case of a H_2/Air-ARC chemistry, the additional complexity introduced by hydrogen requires a more thorough transport model, as it may affect the flame stabilisation mechanism [8]. Otherwise, simpler models may suffice. As for the former, the mixture viscosity is calculated using Wilke's law [28], while individual species viscosities are discerned through kinetic theory [29]. Species thermal conductivities are computed based on Eucken's approach [30], and the thermal conductivity of the mixture is determined using the method of Mathur *et al.* [31]. Lastly, the diffusivities of species are calculated from the Hirschfelder and Curtiss's mixing law [32], where the species binary diffusion coefficients are pre-tabulated as a function of the corresponding operating conditions. For the CH_4 case, a simplified transport model is preferred, where viscosity is calculated using Sutherland's law [33], and the mixture's thermal conductivity is derived from a constant Prandtl number. Additionally, the diffusivity of each species is determined based on a constant Schmidt number.

4.2 Turbulent Combustion Model

The turbulence/flame interaction is modelled using a multi-fuels/hydrogen version of the dynamic TFLES model [34] (otherwise denoted Multi-Fuel TD-TFLES), which has been extended

for thermo-diffusively unstable flames [35] and fuel inhomogeneity caused by multi-components fuels [36]. The model corrects the non-monotonic behaviour of ϕ across the flame front in presence of hydrogen, a behaviour observed when using Bilger's mixture fraction [37] and caused by hydrogen's preferential diffusion. This correction is achieved through an additional passive scalar which tracks down the fuel, thereby resulting in monotonic variations of both z and ϕ for H_2-enriched flames. For compositionally inhomogeneous mixtures, varying diffusion properties across fuel components also alter the local fuel mixture composition. This poses a challenge for accurately parametrising the thickening field, which relies on a reference value lookup table that requires the local equivalence ratio. This challenge is managed by using passive scalars to track each fuel component, allowing retrieval of the local fuel composition while accounting for different diffusion rates. In this context, the implementation of a novel relaxed flame sensor [38], enabling precise differentiation between the hot and cold sides, is needed. This calibration is particularly challenging in reactive zones with a wide range of mixture fractions within, as well as outside, the flammability limits, whose occurrence is typical in industrial partially premixed systems. As for the CH_4 case, Multi-Fuel TD-TFLES is replaced by the classical dynamic TFLES, which relies upon Bilger's mixture fraction to retrieve the local equivalence ratio. All TF implementations require a wrinkling sub-grid scale model, for which Charlette's algebraic model [39] with $\beta = 0.5$ is employed here. In the current study, sub-grid scale wrinkling caused by thermo-diffusive effects are modelled by increasing the local reaction rate in very lean combustion zones. This is achieved by multiplying the sub-grid scale wrinkling by a factor I_0, derived from the DNS performed by Berger *et al.* [40]. The latter is a pragmatic approach, especially in turbulent flows, as the implicit scale separation assumption of the model is not verified and that synergistic effects between TD instabilities and turbulence are neglected. Nonetheless, it is deemed as a first order correction in the TFLES formulation. In the context of TFLES, it is also important to note that the flame response to stretch is overestimated [41]. No specific model has been employed in the present work to address this aspect, which remains a subject for future work. Finally, Takeno index [42] conditioning is used to distinguish premix from diffusion, allowing local thickening exclusively in the premix zones. A summary of chemistry schemes, transport and turbulent combustion models for all cases simulated may be found in Tab. 1.

	Chemistry	Transport	Combustion
CH_4	2S-CH4-BFER	Simplified	TFLES
CH_4/H_2	CH4-15-256-9	Complex	Multi-Fuel-TD
H_2	H2-9-42-0	Complex	Multi-Fuel-TD

TABLE 1: SUMMARY OF CHEMISTRY SCHEME, TRANSPORT MODEL AND TF VERSION.

4.3 Boundary Conditions and Mesh

All cases are simulated using a simplified CAD model of the actual geometry, where mesh-constraining geometrical details are disposed of. For numerical simplification, only a 90-degree sector is modelled, with periodic boundary conditions applied to the sides. The acoustic treatment at the boundaries follows Poinsot & Lele's NSCBC approach [43], while wall boundaries obeys an adiabatic logarithmic law-of-the-wall formulation [44], except for the combustion chamber liner, where heat losses are included by imposing a reference temperature T_{ref} and a suitable thermal resistance R. The air inlet velocity profile, introduced before the swirler and indicated as green cylindrical surface in Fig. 3, is based on velocity data extracted from previous RANS simulations using a detailed CAD model of the burner (refer to [9] for a complete description of the BEV geometry). No turbulence is introduced at the main air inlet, and only velocity profiles, species and temperature are imposed. The presence of the geometrical swirler in the simulation generates sufficient turbulence to be aerodynamically representative of the real burner. Multiple tests show that values of K_{inlet} close to 300 s^{-1} achieve fast convergence to the reference values at the patch and marginal effects of the acoustic waves in terms of reflection. Similarly, a value of K_{outlet} = 100 s^{-1} has been imposed at the outlet. In Fig. 2, the scheme of the fuel injection is shown. In the simulations, fuel injection in both the premix slots and the pilot is included in the CFD geometry and defined as mass flow inlets.

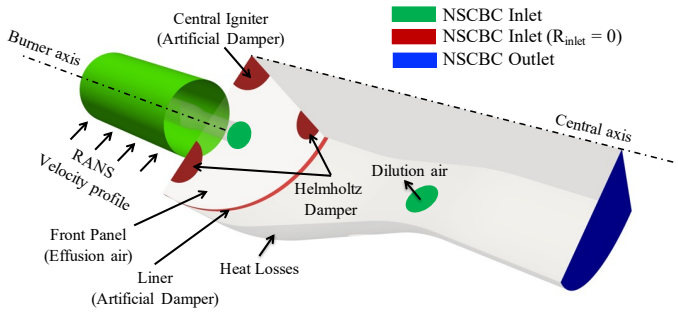

FIGURE 3: 3D REPRESENTATION OF MBFS (SIMPLIFIED) AND MAIN BOUNDARY CONDITIONS. SWIRLER NOT INCLUDED IN THE SCHEME.

As previously mentioned in Sec. 3, for the H_2 case, the PFR is more than 1.5 times than the one of the CH_4/H_2 case. This is achieved by injecting additional fuel into the pilot using the oil injectors in the lance. As noted in [9], this additional injection extends the operational range of the burner. This injection through the oil nozzles is applied only in the H_2 case, with the injectors being geometrically defined and set as mass flow inlets. Throughout the study, a transverse mode was observed, irrespective of the LES numerical setup and initial solution. This instability does not occur during real burner operations. Similar unstable, self-excited transverse modes have been reported in the literature [45–47], often attributed to the use of compressible solvers and the absence of damping at the combustor walls. To address this issue, a similar methodology to that described in [48] is employed. Based on this approach, the premix igniter is replaced with a quasi-zero-velocity inlet at low relaxation coefficient K_{inlet}, making it almost fully non-reflective. By the same token, a 1 cm-long quasi-zero-velocity inlet with low K_{inlet} is implemented near the chamber wedge adjacent to the liner. This allows the trans-

verse mode to evacuate the domain. For distinct purposes, two Helmholtz dampers are placed on the front panel and are modelled likewise. Various tests show no impact of these inlets on the flame dynamics (not shown). Finally, effusion air is injected from the front panel at a uniform gyration angle on the entire plane, according to the formulation of Mendes & Nicoud [49], i.e. an homogeneous condition that injects a prescribed mass flow rate, with an angle different from the geometric angle, in such a way as to reproduce the proper tangential momentum fluxes. The effective angle is calculated from the geometric angle and the porosity of the plate. A schematic representation is depicted in Fig. 3 which sums up the configuration on the front panel. The governing equations are solved on fully unstructured tetrahedral meshes of approximately 35M, 40M, 34M cells for the three different blend ratios, respectively. These are the final results of a mesh-adaptation procedure: across all cases, a first-guess solution on a coarser grid is obtained and used to statically refine the mesh according to physics-based criteria by means of the mesh-adaptation tools Tékigô [50] and MMG3D [51]. The final outcomes are depicted in Fig. 4. The time step is adapted to have a CFL number below 0.9, and is kept above 20 ns thanks to the refinement procedure. After a steady state is reached, the solution is time-averaged over at least 10 convective times with respect to the combustion chamber.

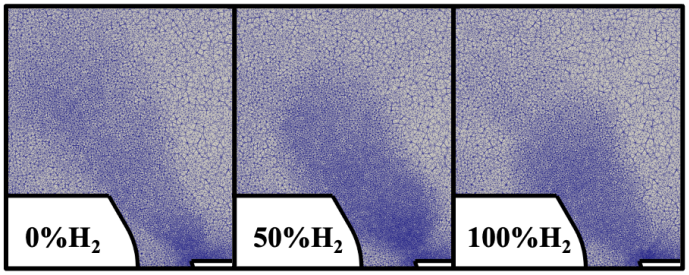

FIGURE 4: LOCAL GRID RESOLUTION FOR ALL CASES.

5. RESULTS

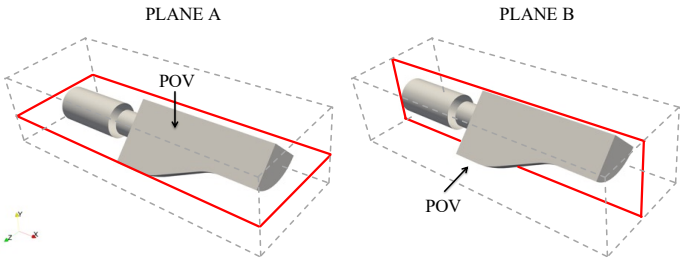

FIGURE 5: ILLUSTRATION OF CROSS-PLANE "A" AND "B" AND RESPECTIVE VIEWING ANGLES.

At the outset, it is helpful to establish definitions for a few key quantities that will be central to the upcoming discussion. By clarifying some of these variables in advance, we ensure a more precise interpretation of the analysis that follows. Normalization is applied to avoid disclosure of confidential information. First, the normalised temperature is defined as:

$$\Theta = \frac{T - T_\mathrm{u}}{T_\mathrm{ad} - T_\mathrm{u}}, \tag{1}$$

where T_ab is the theoretical adiabatic flame temperature at the mean operating premix equivalence ratio ϕ_premix, while T_u is the local time-averaged fresh gas temperature. Likewise, a normalised heat release is written out as:

$$q^* = \frac{q}{\dot{m}_\mathrm{fuel}\Delta H_\mathrm{ref}} = \frac{q}{P_\mathrm{ref}}, \tag{2}$$

where the denominator depends on a reference 1D premix flame representative of the operating conditions. The velocity is normalised by means of the velocity U_0, taken as the average velocity magnitude measured on a cross-plane sufficiently close to the pilot rim, so that:

$$U^* = \frac{|\mathbf{U}|}{U_0}. \tag{3}$$

To differentiate between combustion regimes, a dimensional Flame Index (FI) is utilised [8]:

$$\mathrm{FI}_\mathrm{fuel} = |\dot{\omega}_\mathrm{fuel}| \left. \frac{\nabla Y_\mathrm{fuel} \cdot \nabla Y_{O_2}}{|\nabla Y_\mathrm{fuel} \cdot \nabla Y_{O_2}|} \right|_{\dot{\omega}_\mathrm{fuel}<0} \tag{4}$$

where a conditioning based on the fuel source term $\dot{\omega}_\mathrm{fuel}$ serves to highlight regions of high fuel consumption. As a consequence, negative values shall correspond to a "diffusion" mode, whereas positive values to a "premix" mode. It is important to note that Eq. 4 represents a defined quantity without inherent physical meaning. Although more rigorous formalisms exist [52, 53], which are used to model chemical source terms differently depending on the combustion regime, Eq. 4 is not employed for this purpose. The objective here is not to adopt the most precise definition, but rather to use a post-processing tool to qualitatively distinguish between diffusion and premixing, which might be relevant when transitioning from a pure hydrocarbon to a CH_4/H_2 or pure H_2 mixture. The analysis will primarily focus on two planes: plane "A" corresponds to the symmetry plane of the first stage, spanning the geometry from one periodic side to the other, while plane "B" extends vertically from the top of the geometry down to the combustor liner, representing a middle longitudinal plane. These are illustrated in Fig. 5. In the following, although divided into sections, the three cases are never treated separately and references to the others are made to emphasize major differences.

5.1 Case X_{H_2} = 0 ("CH_4")

The axial velocity field, as depicted in Fig. 6, is not fully symmetric. Specifically, higher negative velocities in the Inner Recirculation Zone (IRZ) are evidenced on one side. Moreover, the swirling jet in the combustion chamber differs on either side. This phenomenon arises primarily from the lack of flow symmetry around the burner axis caused by the combustor geometry contraction (see Fig. 3), as single sector of a multi-burner configuration, compounded by the influence of a swirling flow. Consequently, one cannot expect an aerodynamically stabilised flame to exhibit symmetry in any of the three cases. The velocity field in the combustor chamber clearly changes the flame angle, species

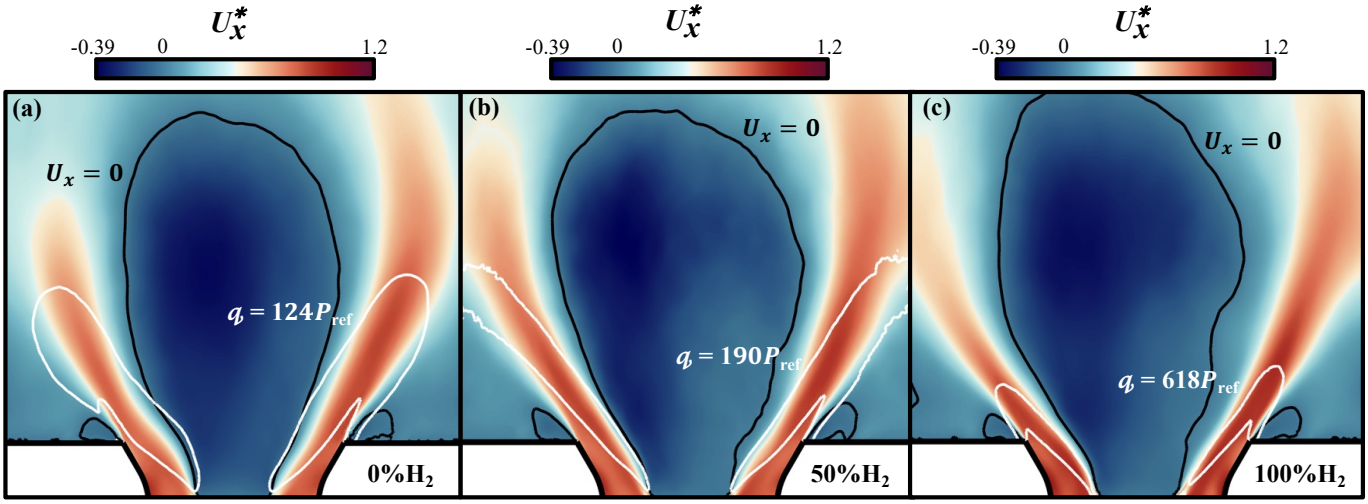

FIGURE 6: AXIAL VELOCITY FIELD ON PLANE "A" ACROSS CASES. THICK WHITE LINES ARE ISOLINES OF 10% q_{max}, WHILE THICK BLACK LINES ARE ISO-CONTOURS OF ZERO AXIAL VELOCITY.

mass fraction distributions, and, consequently, the temperature field, all of which influence the flame stabilisation. The normalized heat release distribution across cases is shown in Fig. 7. At 0% H_2, an M-flame stabilises partially, particularly on the right side (Fig. 7a), with two fronts lying across the Inner Shear Layer (ISL) and Outer Shear Layer (OSL) in the low-velocity region, as shown in Fig. 6. However, the flame never fully stabilises as an M-flame, as illustrated in Fig. 7a. The flame shape is primarily dependent on the propensity of flamelets at the flame tip to propagate through the diluted reactants (by combustion products) in the OSL of the swirling jet, which interacts with the hot Outer Recirculation Region (ORZ). In that respect, the local temperature certainly plays a role. The reason why a M-flame can not stabilise is evidenced by the temperature field near the ORZ (Fig. 8a), which displays a cooler region on the left side. Indeed, a 3D analysis of the region close to the front panel reveals differences in the ORZ, indicating that one side is cooler than the other. This is likely due to the interaction between the flow in the combustion chamber and the effusion cooling on the front panel. Indeed, the swirling motion directs part of the effusion air in the near-liner flow to exit through the adjacent periodic side, before re-entering on the other side and being further pushed toward the liner (not shown). This side effect is purely geometrical and may depend on the adapted effusion modelling applied in the current study. As a result, the average residence time of cooling air in that region increases, maintaining temperatures too low for the reaction to extend further into the OSL and thereby hindering flame stabilisation only in that specific area. It should be noted that this holds true across all cases except for the H_2 case, as shown in Fig. 7c. In fact, hydrogen oxidation occurs at much lower temperatures and equivalence ratios [3] than the other two fuel mixtures, and therefore a M-shape is highly probable. Henceforth, the side where the flame does not stabilise through the OSL will be denoted "V-side" in some instances.

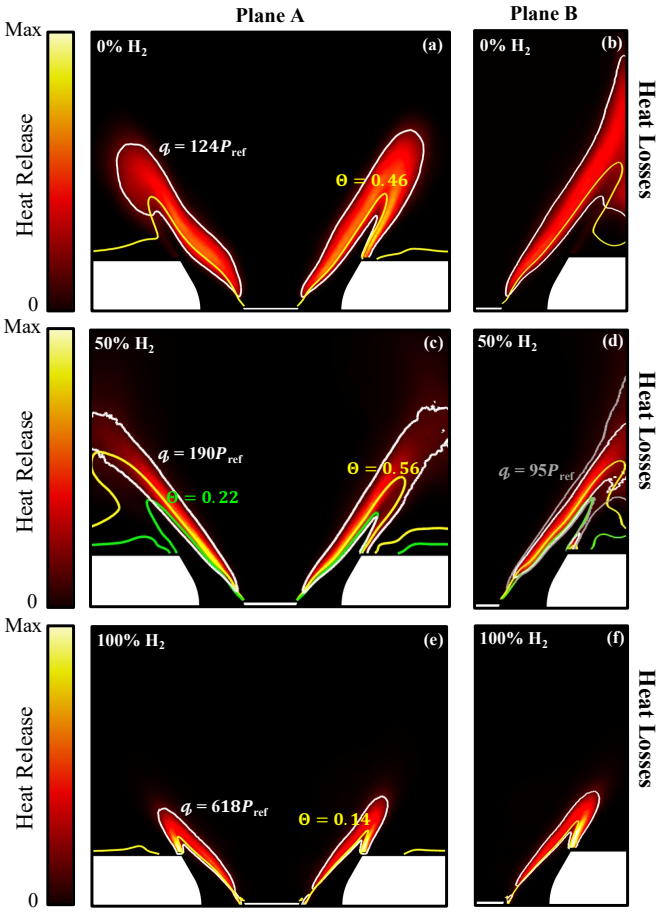

FIGURE 7: (LEFT COLUMN) TIME-AVERAGED HEAT RELEASE DISTRIBUTION ON THE BURNER PLANE "A". (RIGHT COLUMN) TIME-AVERAGED HEAT RELEASE ON PLANE "B" (ZOOM ON CHAMBER LINER). THICK WHITE AND GREY LINES CORRESPOND TO ISOLINES OF 10% q_{max} AND 5% q_{max}, RESPECTIVELY. THICK COLOURED LINES ARE ISO-CONTOURS OF NORMALISED TEMPERATURE. EACH ROW CORRESPONDS TO ONE OF THE THREE SIMULATED CASES.

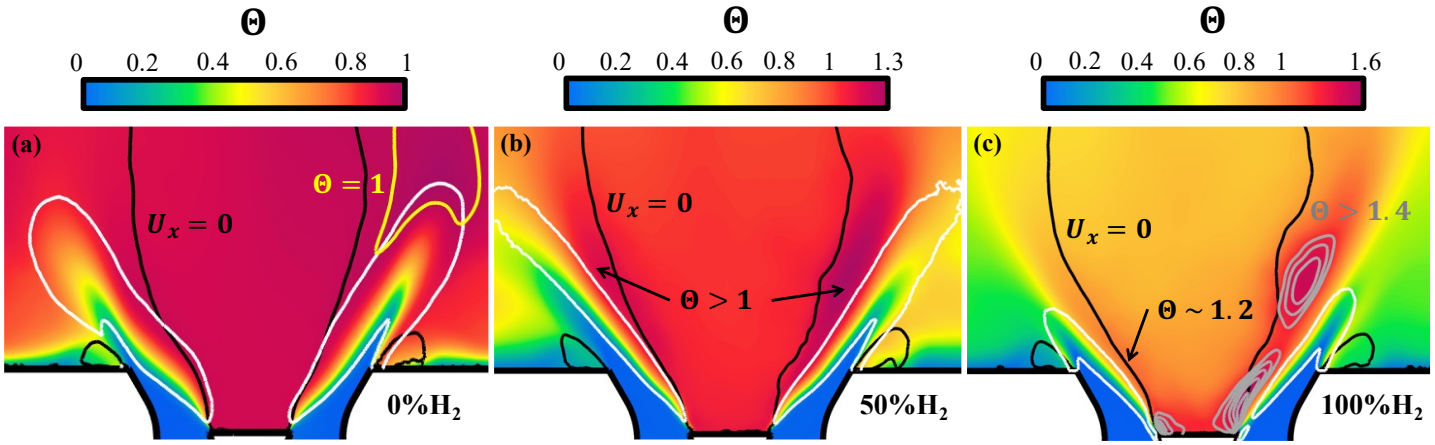

FIGURE 8: TIME-AVERAGED NORMALISED TEMPERATURE FIELD ON CROSS-PLANE "A", ACROSS CASES. THICK BLACK LINES ARE ISO-CONTOURS OF ZERO AXIAL VELOCITY, WHILE THICK WHITE LINES ARE ISOLINES OF 10% q_{max}. IN THE REGION ENCOMPASSED INTO THE YELLOW LINE, Θ ≈ 1, WHILE GREY LINES DELIMITATE AREAS WHERE Θ > 1.4.

To illustrate this point, Fig. 9 shows the normalised oxygen mass fraction, equivalence ratio, and temperature at 5 mm from the front panel on the burner symmetry plane. Higher oxygen content is observed on the "V-side", a result of effusion air exiting on one side and re-entering on the other, as shown in Fig. 9a. This circulation leads, on average, to elevated oxygen levels, which in turn reduce the local equivalence ratio and temperature (Fig. 9b and Fig. 9c).

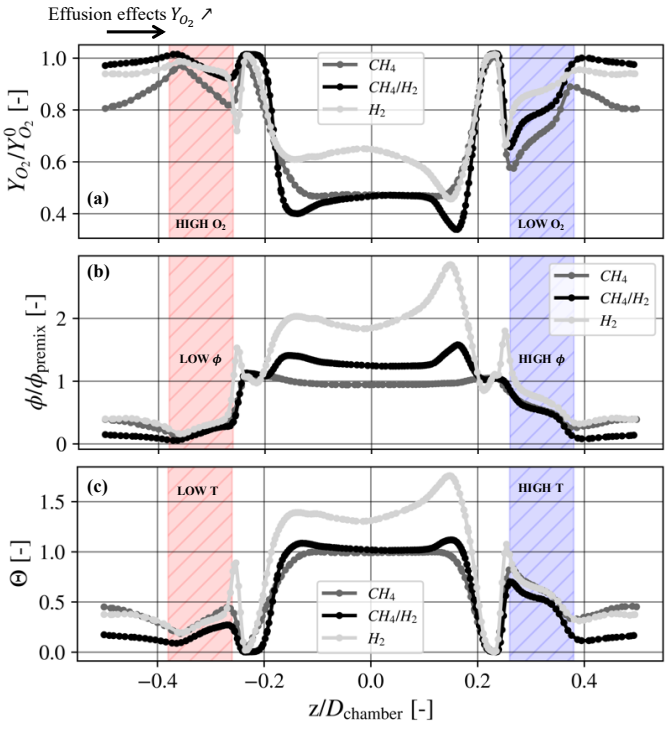

FIGURE 9: NORMALISED TIME-AVERAGED PROFILES OF OXYGEN MASS FRACTION (A), EQUIVALENCE RATIO (B) AND TEMPERATURE (C) AT 5 MM FROM THE FRONT PANEL ON THE CROSS-PLANE "A", SHOWN ACROSS CASES.

It is important to note that the elevated oxygen mass fraction has a dilution effect, making the flame front leaner and lowering the flame temperature. This effect is also evidenced by Fig. 8a, where a broader reaction layer and normalized temperature values slightly below unity are observed on the "V-side". Because of the velocity field asymmetry, the flame tends to stabilise with a different angle around the same area. It is noted that different shapes of the swirling jet also impact the temperature field and therefore change the spatial distribution of heat release. This effect is seen in Fig. 7a, where the temperature isoline at Θ = 0.46, corresponding to the activation temperature of methane oxidation, seems to be slightly distorted. As a consequence, the heat release, aligning with the latter, changes its distribution and the flame shape is impacted. To conclude, Fig. 7b shows the flame in the vicinity of the liner, where heat losses are imposed. The temperature of combustion products in the ORZ is affected, influencing the reaction in the OSL, and thereby preventing stabilisation of the flame in that region [54].

5.2 Case X_{H_2} = 0.5 ("CH_4/H_2")

At 50%$_{vol}$ H_2, the flame morphology exhibits analogous behaviour to the one reported for the CH_4 case. Although qualitatively similar, a few notable distinctions can be identified. First, the temperature differences between the two sides in the ORZ (Fig. 8b), where effusion effects influence the flame stabilisation in the OSL, appear more pronounced. This, combined with a lower overall premix equivalence ratio than the CH_4 case, does not allow combustion to extend through the left-side OSL, presumably due to quenching effects. Consequently, this results in a longer flame on the "V-side" than in the CH_4 case which mainly stabilises in the ISL. Second, similarly to the CH_4 case, a flame front is observed in the OSL region on the right side (Fig. 7c). However, the LES predicts lower values of heat release in that region, compared to the one in the ISL. Indeed, an analysis of the instantaneous 3D field shows that, over time, occasionally in that region, the flame slightly detaches from the front panel, nonetheless keeping the M-shape topology on average. This arises because, while a lower ϕ_{premix} makes a V-flame more likely to stabilise [4], the hydrogen enrichment enhances local reactivity of the mixture, thereby facilitating the forma-

tion of a reaction front in that area. This is particularly true in proximity of the front panel, where hydrogen diffuses rapidly and temperature values are large enough for hydrogen oxidation to occur, as shown by the temperature iso-contour at $\Theta = 0.22$ in Fig. 7c. It is also important to recall that, in this case, the injected hydrogen constitutes only 50% of the mixture volume, resulting in a relatively weak flame front in that region. In addition, the tendency of hydrogen to diffuse very fast and evacuate the premix mixture allows for a weak diffusion front facing the right-side ORZ to form, as shown by Fig. 10a. This front is evidently caused by the reaction between H_2 and recirculating O_2 at moderately low temperatures. Overall, it can be concluded that hydrogen enrichment aids the stabilisation of a M-flame, even when the equivalence ratio is significantly lower, compared to the CH_4 case. This conclusion is coherent with past literature on the topic [4]. Figure 10a shows that most of the CH_3 mass fraction, issued by the dissociation of CH_4, is contained within the heat release iso-contour at 10% q_{max}, delineating the premix flame front. Since CH_3 is a direct product of methane oxidation, this suggests that the mean heat release is primarily driven by CH_4, and not H_2. In contrast, high concentrations of OH are located across the heat release isoline, at the boundary of the IRZ, where temperatures are higher. Figure 10c and Figure 10d illustrate the reaction rates of two high-temperature hydrogen-oxygen shuffle reactions ($H_2 + O \longleftrightarrow H + OH$ and $H + O_2 \longleftrightarrow O + OH$) that govern radical interconversion of H, O, and OH [3]. Initially, H and O are generated in the premix front, then proceed to react with H_2 and O_2 injected from the pilot in a diffusion mode. In other words, hot products originating from the CH_4/air premix react with the pure stream of fuel and air injected from the pilot, creating a diffusion-driven area. This process is highlighted in Fig. 10e, where a distinct diffusion branch is locked into that region. These reactions drive the high OH concentrations previously mentioned, making H_2 the prime contributor for the heat release in this region. It is important to note that CH_4 never burns in a diffusion mode, even though, like hydrogen, it is injected from the pilot, indicating that the high OH production descends extensively from hydrogen's proclivity to unmix thanks to preferential diffusion. Coherently, the temperature field in Fig. 8b reveals the presence of a diffusion kernel through higher local temperatures, indicated by normalized temperature values exceeding unity. Also, the hydrogen enrichment affects the flame stabilisation. As a first observation, Fig. 6b shows a more symmetric swirling jet, resulting in a less impacted temperature field as shown by the isolines of temperature in Fig. 7b. Unlike in the pure CH_4 case, the diffusion branch, stabilising in the low-velocity zone thanks to the higher PFR, enables the premix front to stabilise more easily in the high-velocity region with the exception of the flame root. Figure 8b illustrates the heat release isoline superimposed on the temperature field. The diffusion kernel appears to be the separator between the IRZ and the premix front, keeping the latter locked into the jet, a phenomenon that does not occur with pure CH_4. The flame behaviour in presence of heat losses changes with respect to the CH_4 case. In fact, the presence of hydrogen extends the extinction limit of the mixture, and the temperatures remain high enough for a weak flame front to stabilise in the OSL. This is depicted in Fig. 7d, where the flame front is nailed down within the heat release isoline at 5% q_{max}, and whose distribution aligns with the temperature isoline at $\Theta = 0.22$, delineating the onset of hydrogen oxidation.

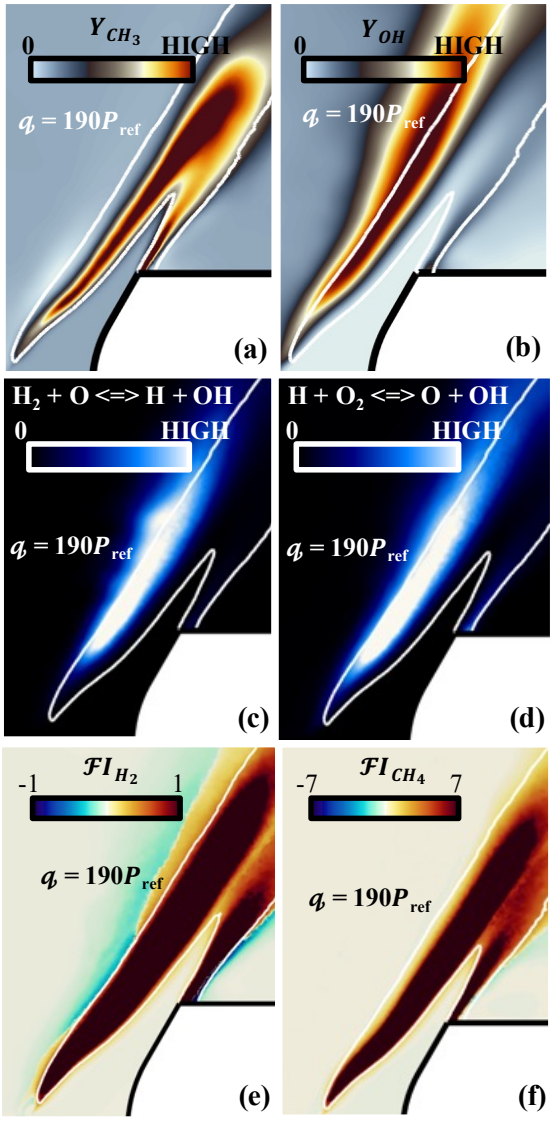

FIGURE 10: TIME-AVERAGED CH3 (A) AND OH (B) MASS FRACTION, TIME-AVERAGED REACTION RATES OF TWO HYDROGEN-OXYGEN SHUFFLE REACTIONS (C-D), AND TIME-AVERAGED DIMENSIONAL TAKENO INDEX (EQ. 4) FOR HYDROGEN (E) AND METHANE (F), ALL PLOTTED ON PLANE "A". THICK WHITE LINES REPRESENT ISOLINES OF 10% q_{max}.

5.3 Case $X_{H_2} = 1$ ("H_2")

When employing pure hydrogen, a compact and short M-flame stabilises in the high-velocity region (Fig. 6c). Hydrogen oxidation occurs at much lower temperatures and equivalence ratios, as is a well-documented characteristic of H_2, attributed to its extended lower flammability limits. Ultimately, the higher reactivity and diffusivity, as well as a lower ignition delay time, ensure that the impact of effusion on the temperature field does not affect the flame shape, unlike in the other two cases. Similarly to the CH_4/H_2 case, hydrogen generates flame fronts facing the

ORZ. Figure 7e illustrates the intense heat release distribution in the OSL, compared to that in the ISL. As expected, hydrogen diffuses rapidly around the diffuser exhaust and reacts in both premix and diffusion modes. The diffusion branch in this region (elucidated in Fig. 11a) is more intense than the one detected in the CH_4/H_2 case and can be attributed to hydrogen evacuating the premix mixture and recirculating oxygen coming from the ORZ. For completeness, the reaction rate of an elementary reaction for HO_2 production involving H_2 and O_2 ($H_2 + O_2 \longleftrightarrow H + HO_2$) is shown in Fig. 11c, which depicts high values in that region. Figure 11a also depicts an intense diffusion kernel at the flame root, and a less intense one at the flame tip, both occurring in the low-velocity region.

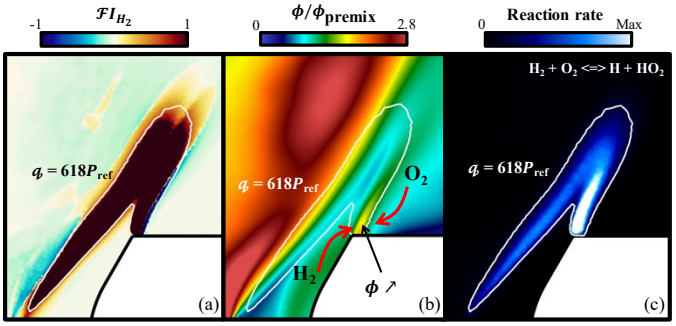

FIGURE 11: (A) TIME-AVERAGED H_2 FLAME INDEX (EQ. 4), (B) TIME-AVERAGED EQUIVALENCE RATIO DISTRIBUTION AND (C) REACTION RATE FOR REACTION $H_2 + O_2 \longleftrightarrow H + HO_2$, PLOTTED ON PLANE "A". THICK WHITE LINES REPRESENT ISOLINES OF 10% q_{max}.

Comparably to the CH_4/H_2 case, this diffusion-driven heat release region arises from high-temperature chemistry between the premixed products and the pilot injection. The recirculation zone, characterized by an asymmetric behaviour (Fig. 6c), combined with a larger PFR, also facilitates hydrogen diffusion and accumulation (Fig. 11b), thus fostering elevated rates of shuffle reactions in that area. As shown in Fig. 12a, high rates of reaction $H + O_2 \longleftrightarrow O + OH$ are produced across the premix front and at the flame root, the latter being the region where the diffusion kernel is locked. This reaction is triggered by recirculating O_2 in the IRZ. As the temperature raises, others more temperature-sensitive hydrogen/oxygen shuffle reactions are promoted, particularly reactions involving the pure H_2 stream injected from the lance pilot and the local composition of the radical pool, such as $H_2 + O \longleftrightarrow H + OH$ and $H_2 + OH \longleftrightarrow H + H_2O$. Indeed, at the flame root high values of reaction rates are observed due to H_2 concentration, as depicted in Fig. 12b and Fig. 12c. This drives the mean concentration of H_2O pockets corresponding to the regions where the normalised temperature exceeds values of 1.4, as shown in Fig. 12d. Notably, the high H_2O concentration is completely absent on the left side. Therefore, the higher increase in PFR at 100% H_2, combined with the swirling flow and an overall tendency of hydrogen to accumulate locally due to preferential diffusion, results in more elevated local temperatures on one side of the cut plane within the inner shear zone, as shown in Fig. 8c. Nevertheless, inspection of the 3D field reveals that similar high localised concentrations of H_2 mass fraction and temperatures due to the pilot injection in the inner shear are seen around the IRZ.

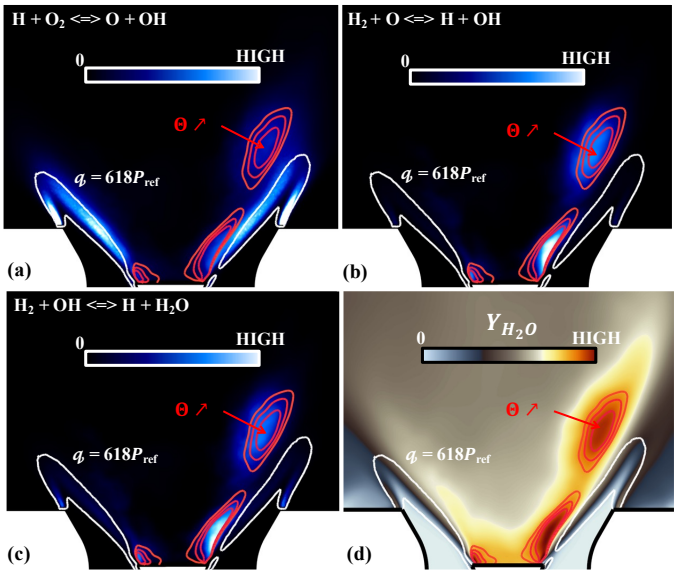

FIGURE 12: TIME-AVERAGED REACTION RATE OF (A) $H + O_2 \longleftrightarrow O + OH$, (B) $H_2 + O \longleftrightarrow H + OH$, (C) $H_2 + OH \longleftrightarrow H + H_2O$ AND (D) TIME-AVERAGED H_2O MASS FRACTION, ALL PLOTTED ON PLANE "A". THICK WHITE LINES REPRESENT ISOLINES OF 10% q_{max}, THICK RED LINES ARE ISOLINE OF TEMPERATURES AT Θ = 1.4, 1.45, 1.5.

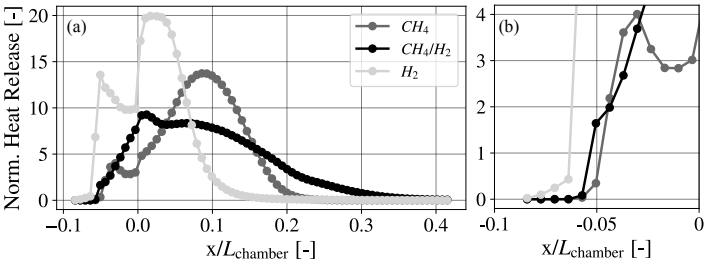

FIGURE 13: (A) AXIAL DISTRIBUTION OF TIME-AVERAGED NORMALISED HEAT RELEASE. (B) ZOOM ON THE PILOT LANCE RIM.

To achieve a more quantitative comparison of all cases, the normalized time-averaged heat release rate fields are integrated over the combustor cross section:

$$q^*_{ax}(x) = \frac{1}{S_c(x)} \iint_{S_c(x)} q^*(x, y, z)\, dy dz. \tag{5}$$

This yields the one-dimensional mean axial distributions presented in Fig. 13a. The impact of hydrogen enrichment on the flame length becomes evident when comparing the CH_4 and H_2 cases: hydrogen results in a higher peak of heat release located further upstream, and an overall more compact flame structure due to higher fuel consumption, despite the lowest flame temperature among the three cases. Conversely, the CH_4/H_2 mixture

shows a smoother and flatter distribution, resulting in a longer flame. This is primarily caused by the effect of the relatively low premix equivalence ratio on a flame which is mostly CH_4-driven. Additionally, Fig. 13b illustrates that the anchoring point shifts upstream as the hydrogen volumetric fraction increases, moving closer to the pilot. For all mixtures evaluated, the flame stabilises at the end of the lance tip.

6. CONCLUSION

This study provides a comprehensive numerical analysis of the flame in the first stage combustor of Ansaldo Energia GT36 under varying hydrogen enrichment levels. The findings reveal a strong dependence of flame morphology and stabilisation mechanism on the fuel composition, with hydrogen enrichment fostering M-shape stabilisation due to higher reactivity and extended flammability limits. As illustrated, the asymmetry in the combustor velocity and temperature fields, produced by geometrical asymmetry around the burner axis, influences the flame shape across all cases, producing a M-shaped configuration on one side and a V-shaped one on the other, though this effect disappears with pure hydrogen. The distinct interplay between premixed and diffusion combustion, particularly in CH_4/H_2 cases, highlights the critical role of hydrogen in shaping the flame structure. These insights emphasise the importance of fuel composition and flow field characteristics in optimising burner performances and achieving desired combustion stability and efficiency, particularly in transitioning to hydrogen-rich or hydrogen-exclusive fuels. To conclude, as mentioned in the "Introduction", this work serves as a foundation for future studies on GT36 first stage. The conclusions presented here mark the first steps in an ongoing research project.

ACKNOWLEDGMENTS

The research work presented in this manuscript was carried out within the FLEX4H2 project. The FLEX4H2 project is supported by the Clean Hydrogen Partnership and its members European Union, Hydrogen Europe and Hydrogen Europe Research (GA 101101427), and the Swiss Federal Department of Economic Affairs, Education and Research, State Secretariat for Education, Research and Innovation (SERI). Views and opinions expressed are however those of the author(s) only and do not necessarily reflect those of the European Union or any other granting authority. Neither of them is liable for any use that may be made of the information contained therein. This work was granted access to the computer resources of CINES and TGCC under the allocation 2024-A0152B10157 made by GENCI.

REFERENCES

[1] Chen, Zheng. "Effects of hydrogen addition on the propagation of spherical methane/air flames: A computational study." *International Journal of Hydrogen Energy* Vol. 34 No. 15 (2009): pp. 6558–6567.

[2] Boushaki, T., Dhué, Y., Selle, L., Ferret, B. and Poinsot, T. "Effects of hydrogen and steam addition on laminar burning velocity of methane–air premixed flame: Experimental and numerical analysis." *International Journal of Hydrogen Energy* Vol. 37 No. 11 (2012): pp. 9412–9422.

[3] Sánchez, Antonio L. and Williams, Forman A. "Recent advances in understanding of flammability characteristics of hydrogen." *Progress in Energy and Combustion Science* Vol. 41 (2014): pp. 1–55.

[4] Guiberti, T.F., Durox, D., Scouflaire, P. and Schuller, T. "Impact of heat loss and hydrogen enrichment on the shape of confined swirling flames." *Proceedings of the Combustion Institute* Vol. 35 No. 2 (2015): pp. 1385–1392.

[5] Zhang, Jianan and Ratner, Albert. "Experimental study on the excitation of thermoacoustic instability of hydrogen-methane/air premixed flames under atmospheric and elevated pressure conditions." *International Journal of Hydrogen Energy* Vol. 44 No. 39 (2019): pp. 21324–21335.

[6] Lim, Zhengli, Li, Jingxuan and Morgans, Aimee S. "The effect of hydrogen enrichment on the forced response of CH4/H2/Air laminar flames." *International Journal of Hydrogen Energy* Vol. 46 No. 46 (2021): pp. 23943–23953.

[7] Pitsch, Heinz. "Large-eddy simulation of turbulent combustion." *Annual Review Fluid Mechanics* Vol. 38 No. 1 (2006): pp. 453–482.

[8] Laera, D., Agostinelli, P.W., Selle, L., Cazères, Q., Oztarlik, G., Schuller, T., Gicquel, L. and Poinsot, T. "Stabilization mechanisms of CH4 premixed swirled flame enriched with a non-premixed hydrogen injection." *Proceedings of the Combustion Institute* Vol. 38 No. 4 (2021): pp. 6355–6363.

[9] Pennell, Douglas, Tay-Wo-Chong, Luis, Smith, Richard, Sierra Sanchez, Patricia and Ciani, Andrea. "GT36 First Stage Development Enabling Load and Fuel (H2) Flexibility With Low Emissions." *Turbo Expo: Power for Land, Sea, and Air*, Vol. Volume 3B: Combustion, Fuels, and Emissions: p. V03BT04A045. 2023.

[10] Pennell, Douglas A., Bothien, Mirko R., Ciani, Andrea, Granet, Victor, Singla, Ghislain, Thorpe, Steven, Wickstroem, Anders, Oumejjoud, Khalid and Yaquinto, Matthew. "An Introduction to the Ansaldo GT36 Constant Pressure Sequential Combustor." *Turbo Expo: Power for Land, Sea, and Air*, Vol. Volume 4B: Combustion, Fuels and Emissions: p. V04BT04A043. 2017.

[11] Ciani, Andrea, Bothien, Mirko R., Bunkute, Birute, Wood, John P. and Früchtel, Gerhard. "Superior fuel and operational flexibility of sequential combustion in Ansaldo Energia gas turbines." *Journal of the Global Power and Propulsion Society* Vol. 3 (2019): pp. 630–638.

[12] Bothien, Mirko R., Ciani, Andrea, Wood, John P. and Fruechtel, Gerhard. "Toward Decarbonized Power Generation With Gas Turbines by Using Sequential Combustion for Burning Hydrogen." *Journal of Engineering for Gas Turbines and Power* Vol. 141 No. 12 (2019): p. 121013.

[13] Sierra Sánchez, P., Pennell, D., Smith, R., Wickström, A., Gant, F. and Boudy, F. "Combustor Operational Flexibility in the Ansaldo Energia GT36 Fleet." *Turbo Expo: Power for Land, Sea, and Air*, Vol. Volume 3B: Combustion, Fuels, and Emissions: p. V03BT04A061. 2024.

[14] Ciani, A., Wood, J. P., Maurer, M., Bunkute, B., Pennell, D., Riazantsev, S. and Früchtel, G. "Center Body Burner for Sequential Combustion: Superior Performance at Lower

Emissions." *Turbo Expo: Power for Land, Sea, and Air*, Vol. Volume 3A: Combustion, Fuels, and Emissions: p. V03AT04A036. 2021. American Society of Mechanical Engineers.

[15] Zajadatz, Martin, Lachner, Rudolf, Bernero, Stefano, Motz, Christian and Flohr, Peter. "Development and Design of Alstom's Staged Fuel Gas Injection EV Burner for NOx Reduction." *Turbo Expo: Power for Land, Sea, and Air*, Vol. Volume 2: Turbo Expo 2007: pp. 559–567. 2007.

[16] Jansohn, Peter, Ruck, Thomas, Steinbach, Christian, Knöpfel, Hans-Peter, Sattelmayer, Thomas and Troger, Christian. "Development of the Advanced EV (AEV) Burner for the ABB GTX100 Gas Turbine." *Turbo Expo: Power for Land, Sea, and Air*, Vol. ASME 1997 Turbo Asia Conference: p. V001T05A009. 1997.

[17] Schönfeld, T. and Rudgyard, M. "Steady and unsteady flow simulations using the hybrid flow solver AVBP." *AIAA journal* Vol. 37 No. 11 (1999): pp. 1378–1385.

[18] Fiorina, B., Vicquelin, R., Auzillon, P., Darabiha, N., Gicquel, O. and Veynante, D. "A filtered tabulated chemistry model for LES of premixed combustion." *Combustion and Flame* Vol. 157 No. 3 (2010): pp. 465–475.

[19] Wolf, P., Staffelbach, G., Roux, A., Gicquel, L., Poinsot, T. and Moureau, V. "Massively parallel LES of azimuthal thermo-acoustic instabilities in annular gas turbines." *Comptes Rendus Mécanique* Vol. 337 No. 6 (2009): pp. 385–394.

[20] Lax, Peter and Wendroff, Burton. "Systems of conservation laws." *Selected Papers Volume I*. Springer (2005): pp. 263–283.

[21] Smagorinsky, Joseph. "General circulation experiments with the primitive equations: I. The basic experiment." *Monthly Weather Review* Vol. 91 No. 3 (1963): pp. 99 – 164.

[22] Franzelli, Benedetta, Riber, Eleonore, Gicquel, Laurent Y.M. and Poinsot, Thierry. "Large Eddy Simulation of combustion instabilities in a lean partially premixed swirled flame." *Combustion and Flame* Vol. 159 No. 2 (2012): pp. 621–637.

[23] Cazères, Quentin, Pepiot, Perrine, Riber, Eleonore and Cuenot, Bénédicte. "A fully automatic procedure for the analytical reduction of chemical kinetics mechanisms for Computational Fluid Dynamics applications." *Fuel* Vol. 303 (2021): p. 121247.

[24] Pestre, Antoine. "Numerical simulations of aeronautical engine ignitions under realistic high altitude conditions." Phd disseration, Institut National Polytechnique de Toulouse - INPT. 2023.

[25] CRECK Modelling Group (Politecnico di Milano). https://creckmodeling.chem.polimi.it.

[26] University of California, San Diego. "Chemical-Kinetic Mechanisms for Combustion Applications." http://combustion.ucsd.edu.

[27] Chapman, S. and Cowling, T.G. *The Mathematical Theory of Non-uniform Gases: An Account of the Kinetic Theory of Viscosity, Thermal Conduction and Diffusion in Gases*. Cambridge Mathematical Library, Cambridge University Press (1990).

[28] Wilke, Charles R. "A viscosity equation for gas mixtures." *The journal of chemical physics* Vol. 18 No. 4 (1950): pp. 517–519.

[29] Bird, R.B., Stewart, W.E. and Lightfoot, E.N. *Transport Phenomena*. No. vol. 1 in *Transport Phenomena*, Wiley (2006).

[30] Eucken, Arnold. "Über das Wärmeleitvermögen, die spezifische Wärme und die innere Reibung der Gase." *Physikalische Zeitschrift* Vol. 14 No. 8 (1913): pp. 324–332.

[31] S. Mathur, P.K. Tondon and Saxena, S.C. "Thermal conductivity of binary, ternary and quaternary mixtures of rare gases." *Molecular Physics* Vol. 12 No. 6 (1967): pp. 569–579.

[32] Hirschfelder, J.O., Curtiss, C.F. and Bird, R.B. *The Molecular Theory of Gases and Liquids*. Wiley (1964).

[33] Sutherland, William. "LII. The viscosity of gases and molecular force." *The London, Edinburgh, and Dublin Philosophical Magazine and Journal of Science* Vol. 36 No. 223 (1893): pp. 507–531.

[34] Colin, O, Ducros, Frédéric, Veynante, D and Poinsot, Thierry. "A thickened flame model for large eddy simulations of turbulent premixed combustion." *Physics of fluids* Vol. 12 No. 7 (2000): pp. 1843–1863.

[35] Aniello, A, Laera, D, Berger, L, Attili, A and Poinsot, T. "Introducing thermo-diffusive effects in large-eddy simulation of turbulent combustion for lean hydrogen-air flames." *Proceedings of the 2022 Summer Program* (2022).

[36] Vargas Ruiz, Héctor José, Laera, Davide, Lartigue, Ghislain and Gicquel, Laurent. "Thickened Flame model for multi-fuel multi-injection combustion." *46th Meeting of the Italian Section of the Combustion Institute*. 2024. Italian Section of the Combustion Institute, Bari, Italy.

[37] Bilger, RW, Stårner, SH and Kee, RJ. "On reduced mechanisms for methane air combustion in nonpremixed flames." *Combustion and Flame* Vol. 80 No. 2 (1990): pp. 135–149.

[38] Jaravel, Thomas. "Prediction of pollutants in gas turbines using large eddy simulation." Theses, Institut National Polytechnique de Toulouse - INPT. 2016.

[39] Charlette, Fabrice, Meneveau, Charles and Veynante, Denis. "A power-law flame wrinkling model for LES of premixed turbulent combustion Part I: non-dynamic formulation and initial tests." *Combustion and Flame* Vol. 131 No. 1 (2002): pp. 159–180.

[40] Berger, Lukas, Attili, Antonio and Pitsch, Heinz. "Intrinsic instabilities in premixed hydrogen flames: Parametric variation of pressure, equivalence ratio, and temperature. Part 1 - Dispersion relations in the linear regime." *Combustion and Flame* Vol. 240 (2022): p. 111935.

[41] Detomaso, Nicola, Hok, Jean-Jacques, Dounia, Omar, Laera, Davide and Poinsot, Thierry. "A generalization of the Thickened Flame model for stretched flames." *Combustion and Flame* Vol. 258 (2023): p. 113080.

[42] Yamashita, H., Shimada, M. and Takeno, T. "A numerical study on flame stability at the transition point of jet diffusion

flames." *Symposium (International) on Combustion* Vol. 26 No. 1 (1996): pp. 27–34.

[43] Poinsot, T.J and Lele, S.K. "Boundary conditions for direct simulations of compressible viscous flows." *Journal of Computational Physics* Vol. 101 No. 1 (1992): pp. 104–129.

[44] Nichols, Robert and Nelson, C. "Wall Function Boundary Conditions Including Heat Transfer and Compressibility." *Aiaa Journal* Vol. 42 (2004): pp. 1107–1114.

[45] Tay Wo Chong, L., Komarek, T., Kaess, R., Foeller, S. and Polifke, W. "Identification of Flame Transfer Functions From LES of a Premixed Swirl Burner." *Turbo Expo: Power for Land, Sea, and Air*, Vol. Volume 2: Combustion, Fuels and Emissions, Parts A and B: pp. 623–635. 2010. American Society of Mechanical Engineers.

[46] Ghani, Abdulla, Poinsot, Thierry, Gicquel, Laurent and Müller, J.-D. "LES Study of Transverse Acoustic Instabilities in a Swirled Kerosene/Air Combustion Chamber." *Flow, Turbulence and Combustion* Vol. 96 No. 1 (2016): pp. 207–226.

[47] Heggset, Tarjei, Meyer, Ole, Tay Wo Chong Hilares, Luis, Ciani, Andrea and Gruber, Andrea. "Numerical Assessment of a Rich-Quench-Lean Staging Strategy for Clean and Efficient Combustion of Partially Decomposed Ammonia in the Constant Pressure Sequential Combustion System." *Journal of Engineering for Gas Turbines and Power* (2023): pp. 1–30.

[48] Eder, Alexander, Silva, Camilo, Häringer, Matthias, Kuhlmann, Johannes and Polifke, Wolfgang. "Incompressible versus compressible large eddy simulation for the identification of premixed flame dynamics." *International Journal of Spray and Combustion Dynamics* Vol. 15 (2023): pp. 16–32.

[49] Mendez, Simon and Nicoud, Franck. "Adiabatic Homogeneous Model for Flow Around a Multiperforated Plate." *AIAA Journal* Vol. 46 No. 10 (2008): pp. 2623–2633.

[50] CERFACS, COOP Team. "Tekigo." http://opentea.pg.cerfacs.fr/tekigo/ (2023). Availability: Dec. 2023.

[51] Dobrzynski, C. "MMG3D: User Guide." Technical Report RT-0422. INRIA. 2012.

[52] Fiorina, B., Gicquel, O., Vervisch, L., Carpentier, S. and Darabiha, N. "Approximating the chemical structure of partially premixed and diffusion counterflow flames using FPI flamelet tabulation." *Combustion and Flame* Vol. 140 No. 3 (2005): pp. 147–160.

[53] Knudsen, E. and Pitsch, H. "A general flamelet transformation useful for distinguishing between premixed and non-premixed modes of combustion." *Combustion and Flame* Vol. 156 No. 3 (2009): pp. 678–696.

[54] Guiberti, Thibault F., Durox, Daniel, Zimmer, Laurent and Schuller, Thierry. "Analysis of topology transitions of swirl flames interacting with the combustor side wall." *Combustion and Flame* Vol. 162 No. 11 (2015).